Correspondence

Carrier Frequency Offset Estimation for OFDM Systems Over Mobile Radio Channels

A. Al-Dweik, *Senior Member, IEEE*, A. Hazmi, *Member, IEEE*, S. Younis, *Student Member, IEEE*, B. Sharif, *Senior Member, IEEE*, and C. Tsimenidis, *Member, IEEE*

***Abstract*—In this paper, a new technique is proposed for blind estimation of carrier frequency offset (CFO) in wireless orthogonal frequency-division multiplexing (OFDM) systems with constant-modulus constellations. The proposed scheme is based on the assumption that the channel slowly changes in the time domain with respect to the OFDM symbol duration. As a consequence, the channel effect on a given subcarrier in two consecutive OFDM symbols is approximately the same. Based on this assumption, a cost function is derived such that the power difference between all subcarriers in two consecutive OFDM symbols is minimized. Using Monte Carlo simulation, we demonstrate that the proposed scheme has superior performance in both static and time-varying frequency-selective fading channels. The proposed system can rapidly and accurately estimate the CFO using only three trial values, given that the CFO is less than half of the subcarriers' frequency spacing.**

***Index Terms*—Blind estimation, Doppler shift, frequency domain, frequency offset, frequency selective, orthogonal frequency-division multiplexing (OFDM), time domain.**

I. Introduction

Orthogonal frequency-division multiplexing (OFDM) is a multicarrier modulation technique that has received remarkable recognition among other digital modulation schemes. The substantial recent interest in OFDM is mainly driven by the increasing demand for robust and bandwidth-efficient modulation schemes to cope with the accelerating expansion and convergence of various wireless networks with very high data rates. The overlapping of the subcarriers' spectra has significantly increased the bandwidth efficiency of OFDM systems with respect to single-carrier systems. Moreover, the unique structure of the OFDM spectrum and the introduction of the time-domain guard band, which is known as the cyclic prefix (CP), has significantly improved the OFDM immunity against multipath propagation effects because each subcarrier suffers from flat fading, even though the overall signal spectrum may suffer from a highly frequency-selective fading process. Consequently, OFDM has been considered for several applications and standards such as IEEE802.11a, IEEE802.16, IEEE802.20, and IEEE802.11n [1]. Moreover, OFDM has been integrated in several other applications such as digital audio broadcasting and digital terrestrial video broadcasting (DVB) in Europe and Japan [2], [3].

Manuscript received April 15, 2009; revised June 27, 2009 and August 13, 2009. First published October 13, 2009; current version published February 19, 2010. The review of this paper was coordinated by Dr. C. Cozzo.

A. Al-Dweik is with the Department of Communications Engineering, Khalifa University of Science, Technology and Research, Sharjah, United Arab Emirates, and also with the School of Electrical, Electronic, and Computer Engineering, Newcastle University, NE1 7RU Newcastle upon Tyne, U.K. (e-mail: dweik@fulbrightmail.org).

A. Hazmi is with the Department of Communications Engineering, Tampere University of Technology, 33720 Tampere, Finland (e-mail: ali.hazmi@tut.fi).

S. Younis, B. Sharif, and C. Tsimenidis are with the School of Electrical, Electronic, and Computer Engineering, Newcastle University, NE1 7RU Newcastle upon Tyne, U.K. (e-mail: s.b.t.younis@ncl.ac.uk; bayan.sharif@ncl.ac.uk; charalampos.tsimenidis@ncl.ac.uk).

Digital Object Identifier 10.1109/TVT.2009.2034169

OFDM signal synchronization consists of two major components, namely, symbol timing recovery and carrier frequency offset (CFO) estimation. The symbol timing offset results from the unknown delay between the transmitter and the receiver. Doppler shifts and the noncoherent up and down frequency conversion performed at the transmitter and receiver, respectively, are the main causes of the CFOs. Based on the CP length and channel parameters, OFDM systems can usually tolerate certain symbol timing errors. However, the requirements for CFO estimates are tighter, and CFOs must accurately be estimated and compensated prior to the discrete Fourier transform (DFT) process. CFOs destroy the subcarriers' orthogonality and create intercarrier interference (ICI) [4], [5]. OFDM systems are highly sensitive to CFOs and can tolerate offsets that are only a fraction of the frequency spacing between the subcarriers without a large degradation of the system SNR [6]. As a consequence, an increasing number of research studies have been dedicated to deriving efficient synchronization techniques for OFDM systems.

In the literature, several blind schemes have been proposed for CFO synchronization of OFDM systems. Some of these techniques, such as the well-referred CP-based estimator (CPE) [7], operate in the time-domain, and the estimation is performed prior to the DFT. In general, the performance of such techniques deteriorates in frequency-selective fading channels [8], [9]. Alternatively, frequency-domain techniques that perform the estimation after the DFT are considered to be more robust. However, they require more computational power. Frequency-domain techniques exploit the DFT output to construct CFO estimators [5], [8]–[11]. In [5], a CFO estimator is proposed that minimizes the variance of the ICI, which is proportional to the CFO. The main drawback of this technique is the modest performance in frequency-selective channels. The estimators proposed in [8] and [11] are based on the modified Viterbi-and-Viterbi algorithm, where the CFO is directly estimated as the phase difference between subcarriers in two consecutive OFDM symbols. In this sense, these estimators can be considered as hybrid time–frequency-domain estimators. The main drawback of these estimators is their limited estimation range, which is inversely proportional to the modulation order, and their high sensitivity to Doppler shifts. In [9], the kurtosis metric, which measures the Gaussianity of a random sequence, is used to construct a kurtosis-type cost function for fine CFO estimation. As will be shown later in this paper, the kurtosis-type estimator and the variance-based estimator are linearly related. Hence, they have the same modest performance. Minimizing the power difference between adjacent subcarriers was used in [10] to develop an efficient CFO estimator. Although this estimator outperforms the variance-based estimator, the CPE, and the kurtosis-type estimator, its performance highly depends on the channel-fading conditions and drastically degrades in highly frequency-selective fading channels [10]. However, the schemes proposed in [9] and [10] have the advantage of being given in closed form, which reduces their computational complexity.

The reason for the degraded performance of the previously mentioned frequency-domain techniques at medium and high SNRs is the fact that the channel selectively fades with respect to the overall OFDM signal spectrum. The assumption that adjacent subcarriers have equal frequency responses is more accurate in fading channels with small delay spreads. This actually becomes apparent at high SNRs, where the difference between the subchannels' frequency response causes the mean square error (MSE) to saturate and creates an error floor [9], [10]. Moreover, the variance and kurtosis-type estimators involve

all subcarriers in the estimation process, which makes them more sensitive to frequency-selective fading as compared with the estimator described in [10], which simply uses the difference between adjacent subcarriers. This has motivated us to propose a new CFO estimator that has high immunity against frequency-selective fading channels by utilizing the time-domain and frequency-domain signals to estimate the CFOs.

In this paper, we propose a low-complexity technique for blind CFO estimation of OFDM systems with constant-modulus (CM) constellations over frequency-selective Rayleigh fading channels. The proposed technique is totally blind and requires no prior knowledge of the channel-state information or the SNR. The proposed estimator, which is denoted as the power difference estimator (PDE), is based on the assumption that the channel slowly changes over two consecutive OFDM symbols. The cost function for the PDE is constructed by minimizing the power difference between all subcarriers in two consecutive OFDM symbols. In this sense, the PDE is a hybrid time–frequency-domain estimator. Unlike other time–frequency-domain CFO estimators, the novel structure of the PDE enables highly accurate estimates over a wide range of SNRs and under severe fading scenarios. The performance of the proposed estimator is evaluated over various channel models including static, slow, and fast frequency-selective fading channels with various degrees of frequency selectivity. The PDE has low complexity because it can efficiently be implemented using the three-point curve-fitting approach described in [9] and [10] as long as the CFO is less than half of the subcarriers' frequency spacing. The performance of the PDE is evaluated by assuming perfect timing synchronization, which is a common assumption for most CFO estimation techniques [8]–[11].

The remainder of this paper is organized as follows. The OFDM system model is presented in Section II. Section III describes the proposed CFO estimator. Numerical results and conclusions are given in Sections IV and V, respectively.

The notation to be used in this paper is defined as follows: Uppercase bold symbols will be used to denote matrices, lowercase bold symbols will denote row or column vectors, $(.)^T$ will denote the transpose, $(.)^*$ will denote the conjugate, $(.)^{-1}$ will denote the inverse, $E[.]$ will denote the average, and $(.)^H$ will denote the Hermitian transpose.

II. Orthogonal Frequency Division Multiplexing System Model

In OFDM systems, a sequence of N complex data symbols is used to modulate N orthogonal subcarriers during the lth OFDM block $\mathbf{d}(l) = [d_0(l), d_1(l), \ldots, d_{N-1}(l)]^T$. The data symbols d_i are usually uniformly drawn from a quadratic-amplitude-modulation or multiple-phase-shift-keying constellation. The sequence of data symbols is modulated using an N-point inverse-DFT (IDFT) process that produces the sequence $\mathbf{x}(l) = [x_0(l), x_1(l), \ldots, x_{N-1}(l)]^T$. Thus

$$\mathbf{x}(l) = \mathbf{W}\mathbf{d}(l) \tag{1}$$

where $\mathbf{W}$ is the normalized $N \times N$ IDFT matrix. The elements of $\mathbf{W}$ are defined as $W_{i,k} = (1/\sqrt{N})\exp(j2\pi ik/N)$, where i and k denote the row and column numbers $\{i, k\} = 0, 1, \ldots, N-1$, respectively. Consequently, the nth sample in the sequence $\mathbf{x}(l)$ can be expressed as

$$x_n(l) = \frac{1}{\sqrt{N}} \sum_{i=0}^{N-1} d_i(l) e^{j2\pi in/N}, \qquad n = 0, 1, \ldots, N-1. \tag{2}$$

In dispersive channels, a time-domain guard interval, which is denoted as the CP, is created by copying the last N_g samples of the IDFT output and appending them at the beginning of the symbol to be transmitted. Therefore, the transmitted OFDM block consists of $N_t = N + N_g$ samples. The useful part of the OFDM symbol does not include the N_g prefix samples and has a duration of T_u seconds.

At the receiver front end, the received signal is applied to a matched filter and then sampled at a rate $T_s = T_u/N$. After dropping the first N_g CP samples, the received sequence $\mathbf{y}(l) = [y_0(l), \ldots, y_{N-1}(l)]^T$ is obtained [9]

$$\mathbf{y}(l) = e^{j\frac{2\pi}{N}\epsilon l(N+N_g)}\mathbf{C}(\epsilon)\mathbf{W}\mathbf{H}(l)\mathbf{d}(l) + \mathbf{z}(l) \tag{3}$$

where ϵ represents the normalized CFO $\epsilon \in (-0.5, 0.5)$, and $\mathbf{C}(\epsilon)$ represents the effect of the accumulated phase shift caused by the CFO on the time-domain samples

$$\mathbf{C}(\epsilon) = \operatorname{diag}\left(\left[e^{\frac{j2\pi\epsilon}{N}\times 0}, e^{\frac{j2\pi\epsilon}{N}\times 1}, \ldots, e^{\frac{j2\pi\epsilon}{N}\times(N-1)}\right]^T\right). \tag{4}$$

$\mathbf{H}(l)$ denotes the channel frequency response during the lth OFDM block

$$\mathbf{H}(l) = \operatorname{diag}\left([H_0(l), H_1(l), \ldots, H_{N-1}(l)]^T\right).$$

$\mathbf{z}(l) = [z_0(l), z_1(l), \ldots, z_{N-1}(l)]^T$ denotes the system noise, which is modeled as a white Gaussian process with zero mean and variance $\sigma_z^2 = E[|z_n|^2]$, and the leading term in (3) represents the effect of the common phase shift. Assuming that the receiver sampling clock is aligned to that of the transmitter, the nth element of $\mathbf{y}(l)$ can be expressed as

$$y_n(l) = \frac{e^{j\frac{2\pi}{N}\epsilon l(N+N_g)}}{\sqrt{N}} \sum_{i=0}^{N-1} d_i(l)H_i(l)e^{j\frac{2\pi n}{N}(i+\epsilon)} + z_n(l). \tag{5}$$

The sequence $\mathbf{y}(l)$ is multiplied by $\mathbf{C}^*(\hat{\epsilon})$ to compensate for the CFO; then, it is fed to the DFT that produces the sequence $\mathbf{s}(l) = [s_0(l), s_1(l), \ldots, s_{N-1}(l)]^T$

$$\mathbf{s}(l) = \mathbf{W}^H\mathbf{C}^*(\hat{\epsilon})\mathbf{y}(l) \tag{6}$$

where $\hat{\epsilon}$ is the estimated value of ϵ. Note that $\mathbf{W}^{-1} = \mathbf{W}^H$ because $\mathbf{W}$ is a unitary matrix. The kth element of $\mathbf{s}(l)$ can be expressed as

$$s_k(l) = \frac{1}{\sqrt{N}} \sum_{n=0}^{N-1} y_n(l)e^{-j\frac{2\pi n}{N}(k+\hat{\epsilon})}. \tag{7}$$

III. Carrier Frequency Offset Estimation for Orthogonal Frequency Division Multiplexing Systems

A. Proposed CFO Estimator

If the CFO is perfectly estimated and compensated, i.e., $\hat{\epsilon} = \epsilon$, then $\mathbf{C}(\epsilon)\mathbf{C}^*(\hat{\epsilon}) = \mathbf{I}$, which is the $N \times N$ identity matrix, and the DFT output for the noise-free case is expressed as

$$\mathbf{s}(l)|_{\hat{\epsilon}=\epsilon} = \mathbf{H}(l)\mathbf{d}(l). \tag{8}$$

In this case, the power of the kth DFT output can be expressed as

$$\left| s_k(l)|_{\hat{\epsilon}=\epsilon} \right|^2 = |H_k(l)|^2 |d_k(l)|^2. \tag{9}$$

Moreover, if the data symbols d_k are selected from a CM constellation and all subcarriers have equal power, then (9) is reduced to [10]

$$\left| s_k(l)|_{\hat{\epsilon}=\epsilon} \right|^2 = |H_k(l)|^2. \tag{10}$$

This is because the power of normalized CM signals is equal to one. Under the assumption that the channel-frequency response parameters $H_k(l)$ slowly change in the time domain with respect to T_u

$$\left| s_k(l)|_{\hat{\epsilon}=\epsilon} \right|^2 \approx |s_k(l-1)_{\hat{\epsilon}=\epsilon}|^2 . \tag{11}$$

When $\hat{\epsilon} \neq \epsilon$, ICI will be introduced at the DFT output [6], and the approximation described in (11) is no longer valid. Therefore, by noting that (11) is valid for all subcarriers, the value of ϵ can be estimated by minimizing the following cost function:

$$J(\tilde{\epsilon}) = \sum_{l=1}^{L} \sum_{k=0}^{N-1} \left(|s_k(l)|^2 - |s_k(l-1)|^2 \right)^2 \tag{12}$$

where $\tilde{\epsilon}$ is the trial value of ϵ, and L represents the number of times that the cost function is averaged in each estimation process. Therefore, the estimates of ϵ, which are denoted as $\hat{\epsilon}$, can be obtained by minimizing the cost function given in (12)

$$\hat{\epsilon} = \underset{\tilde{\epsilon} \in (-0.5, 0.5)}{\arg \min} J(\tilde{\epsilon}). \tag{13}$$

Following a procedure similar to the one described in [10], the cost function $J(\tilde{\epsilon})$ can be approximated by (see the Appendix)

$$J(\tilde{\epsilon}) \approx A \cos\left[2\pi(\epsilon - \tilde{\epsilon})\right] + C \tag{14}$$

where A and C are constants with real values and independent of $\tilde{\epsilon}$ and ϵ. In addition, the results of [10] can be used to show that the cost function of the estimator reported in [5] can be described by (14) as well. Since the cost function described in (12) is sinusoidal, the minimization process, which is usually performed using methods such as the line search or the gradient descent, can be replaced by the curve-fitting method [9], [10]. The curve-fitting method leads to a closed-form estimation of ϵ by evaluating (14) at three special trial points, namely, $\tilde{\epsilon} = -1/4, 0, 1/4$. Then, $\hat{\epsilon}$ can be obtained as

$$\hat{\epsilon} = \begin{cases} \frac{1}{2\pi} \tan^{-1}(b/a), & a \geq 0 \\ \frac{1}{2\pi} \tan^{-1}(b/a) + \frac{1}{2}, & a < 0 \text{ and } b \geq 0 \\ \frac{1}{2\pi} \tan^{-1}(b) - \frac{1}{2}, & a < 0 \text{ and } b \leq 0 \end{cases} \tag{15}$$

where $a \triangleq (1/2)[J(\tilde{\epsilon} = 1/4) + J(\tilde{\epsilon} = -1/4)] - J(\tilde{\epsilon} = 0)$, and $b \triangleq (1/2)[J(\tilde{\epsilon} = 1/4) - J(\tilde{\epsilon} = -1/4)]$.

Although the cost functions reported in (12) and [10] have some similarity, their performance is remarkably different as the discrepancy in the cost functions results from the new dimension, i.e., the time domain that is included in the cost function in (12). However, such similarity implies that both schemes have equivalent complexity. The main difference in complexity between the estimators described in (12) and [10] is that (12) requires computation of the power of the DFT output over two consecutive OFDM blocks instead of one, as in the case of [10].

B. Estimators in [5] and [9]

Unlike the PDE and the estimator in [10], the estimators in [5] and [9], which are denoted as $J_{\mathrm{var}}(\tilde{\epsilon})$ and $J_{\mathrm{kurt}}(\tilde{\epsilon})$, respectively, have similar cost functions and similar performance. To show the similarity of the cost functions, note that, for $L \gg 1$, $J_{\mathrm{kurt}}(\tilde{\epsilon})$ can be expressed as

$$J_{\mathrm{kurt}}(\tilde{\epsilon}) \approx \frac{\sum_{k=0}^{N-1} E\left[|s_k(l)|^4\right]}{\left(\sum_{k=0}^{N-1} E\left[|s_k(l)|^2\right]\right)^2}. \tag{16}$$

In this case, the denominator in (16), which is denoted as K, represents the total energy of the noise-free signal, which is a constant independent of $\tilde{\epsilon}$ [9]. Thus, for $L \gg 1$, $J_{\mathrm{var}}(\tilde{\epsilon})$ can be expressed as

$$J_{\mathrm{var}}(\tilde{\epsilon}) \approx \frac{1}{N} \sum_{k=0}^{N-1} E\left[|s_k(l)|^4\right] - \frac{K}{N^2}. \tag{17}$$

Therefore, the two cost functions have the relation

$$J_{\mathrm{var}}(\tilde{\epsilon}) = \frac{K}{N} J_{\mathrm{kurt}}(\tilde{\epsilon}) - \frac{K}{N^2}. \tag{18}$$

From (18), it can be noted that $J_{\mathrm{var}}(\tilde{\epsilon})$ is an affine transform of $J_{\mathrm{kurt}}(\tilde{\epsilon})$. Moreover, since the two cost functions have a sinusoidal shape and the estimation is performed using the curve-fitting approach given in (15), we conclude that the performance of both algorithms is the same. This conclusion can be confirmed by comparing the results presented in Section IV with those reported in [10].

IV. Numerical Results

The system performance is assessed using Monte Carlo simulation over additive white Gaussian noise (AWGN) and frequency-selective multipath fading channels. In each simulation run, 10^6 OFDM symbols are used. The performance is evaluated by means of normalized MSE, where the MSE of the CFO estimates is normalized with respect to the subcarriers' frequency spacing. The OFDM system considered in this paper has $N = 64$ subcarriers modulated using quaternary phase-shift keying, $N_g = 16$, the subcarriers' data rate is 4.17 kb/s, and the carrier frequency is equal to 2.2 GHz.

For comparison purposes, the channel models used in this paper are the ones reported in [10], which consist of three fading channels. Channel 1 has five paths with delays of [0, 1, 2, 3, 4] samples, average gains of [0.35, 0.25, 0.18, 0.13, 0.09], and mean square delay spread $\sigma^2(\tau) = 1.74$. The mean square delay spread is defined as [13]

$$\sigma^2(\tau) = \frac{\sum_i g_i \tau_i^2}{\sum_i g_i} - \left(\frac{\sum_i g_i \tau_i}{\sum_i g_i} \right)^2 \tag{19}$$

where g_i is the average gain, and τ_i is the delay of the ith path, respectively. Channel 2 also has five paths with delays of [0, 1, 2, 6, 11] samples, average gains of [0.34, 0.28, 0.23, 0.11, 0.04], and $\sigma^2(\tau) = 6.37$. Channel 3 has four paths with delays of [0, 4, 8, 12] samples, gains of [0.25, 0.25, 0.25, 0.25], and $\sigma^2(\tau) = 20$. The path gains are generated as complex independent stochastic variables and the fading with Jakes' Doppler spectrum. The MSE of the proposed PDE is compared with the MSE of the estimators in [5], [9], and [10]. Because the cost functions of these estimators have a sinusoidal shape, all MSE results are obtained using (15).

The MSE of the considered estimators over AWGN channels is depicted in Fig. 1. It can be seen that the MSE of all estimators approximately linearly decreases for SNR $\gtrsim 8$ dB, except for the estimator in [10], which exhibits a slight flatness at high SNRs. While the estimators in [5], [9], and [10] and the PDE have demonstrated an equivalent MSE, the estimator in [7] outperforms all other estimators by about 4 dB.

To evaluate the MSE in moderate frequency-selective fading channels, we use channels 1 and 2, which have mean square delay spreads $\sigma^2(\tau) = 1.74$ and $\sigma^2(\tau) = 6.37$, respectively. As demonstrated in Fig. 2, the PDE outperforms all other systems for the entire range of SNRs over both channels for zero Doppler shifts, i.e., $f_d = 0$. The MSE difference becomes substantial at high SNRs where the MSE of all other considered estimators saturates and becomes flat. The robustness of the PDE against frequency selectivity can be observed

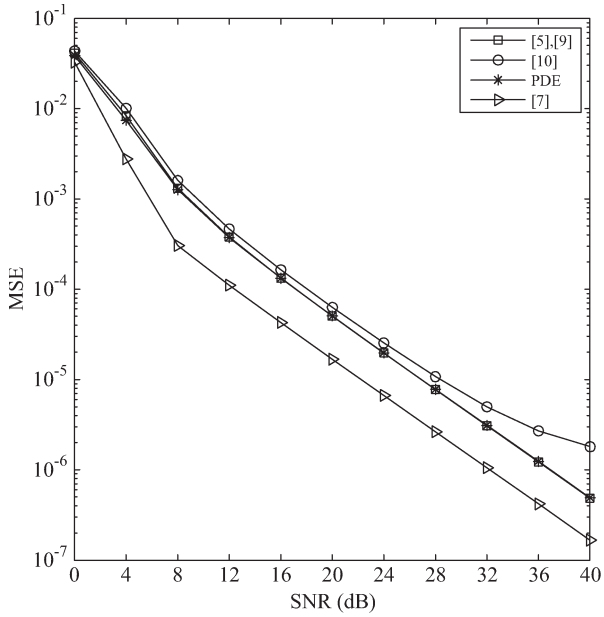

Fig. 1. MSE versus the SNR over AWGN channels: $L = 1$.

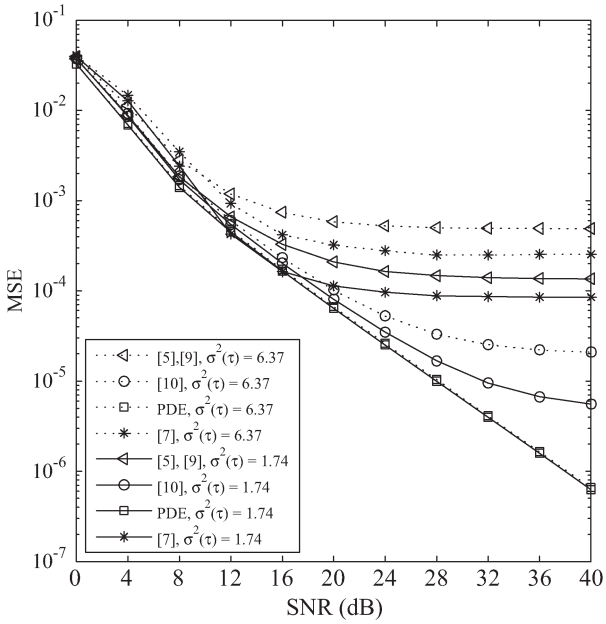

Fig. 2. MSE versus the SNR for frequency-selective fading channels with different delay spreads, $L = 1$, and $f_d = 0$.

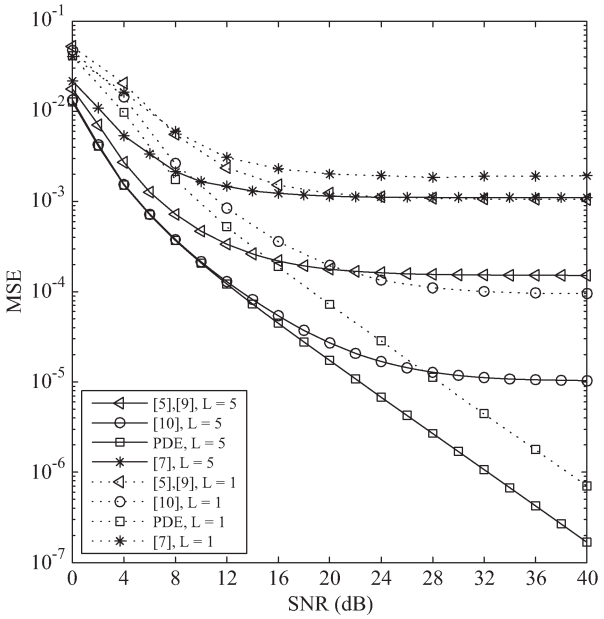

Fig. 3. MSE versus the SNR using $L = 1, 5$, $\sigma^2(\tau) = 20$, and $f_d = 0$.

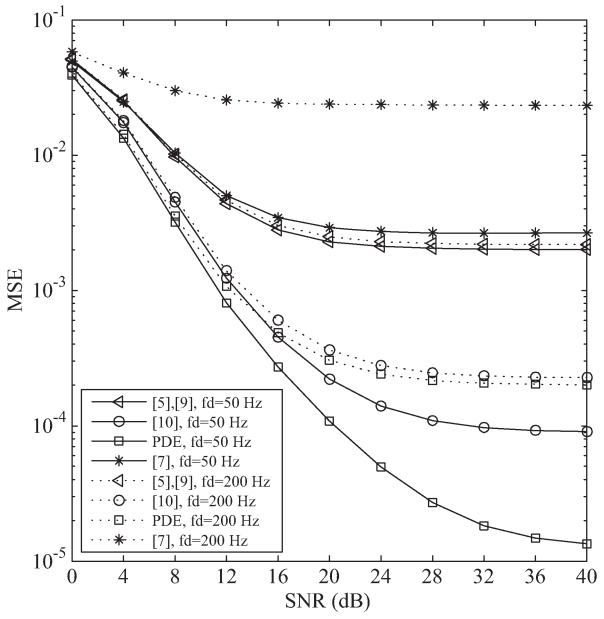

Fig. 4. MSE versus the SNR for different Doppler shift values, $L = 1$, $\sigma^2(\tau) = 20$, $f_d = 50$, and 200 Hz.

from the negligible MSE difference over both channels. The MSE of the estimator in [10] significantly deteriorates when the channel delay spread increases. Similar MSE deterioration has been observed for all the considered systems, except for the PDE. The variance-based estimator is the most vulnerable to large delay spreads at moderate and high SNRs.

The MSE performance over highly frequency-selective static channels is depicted in Fig. 3, where $\sigma^2(\tau) = 20$, and $f_d = 0$. This figure clearly shows the high immunity of the proposed PDE against severe multipath fading conditions. While the MSE of all the considered estimators starts to saturate at SNR $\gtrsim$ 20 dB, the MSE of the PDE continues to decrease by increasing the SNR approximately in a linear manner. Moreover, the MSE of the PDE using $L = 1$ is much smaller than the MSE of the estimator in [10] at high SNRs, even for the $L = 5$ case. Therefore, no averaging is needed for the PDE, even under severe frequency-selective fading conditions.

To evaluate the MSE performance of the proposed system over time-varying frequency-selective fading channels, we consider two different maximum Doppler shifts, namely, 50 and 200 Hz, which correspond to vehicle speeds of approximately 24.5 and 98 km/h, respectively. The channel-3 model is used when $\sigma^2(\tau) = 20$. As depicted in Fig. 4, the PDE still outperforms all the other considered estimators. The MSE of the PDE and that of the estimator in [10] start to converge for vehicle speeds $\gtrsim$ 100 km/h, which is an evidence that the PDE maintains its efficiency even in time-varying channels. Fig. 4 also shows that the MSE of variance-/kurtosis-based estimators does not drastically change as a function of f_d. The CPE seems to be the most sensitive to Doppler shifts as the MSE considerably increases for large f_d values.

The MSE performance of the proposed system versus f_d is presented in Fig. 5 for SNR $= 40$ dB using channels 1 and 3. This figure is used to compare the performance of the PDE and the estimators in [10] and [11] under various levels of frequency selectivity with a wide

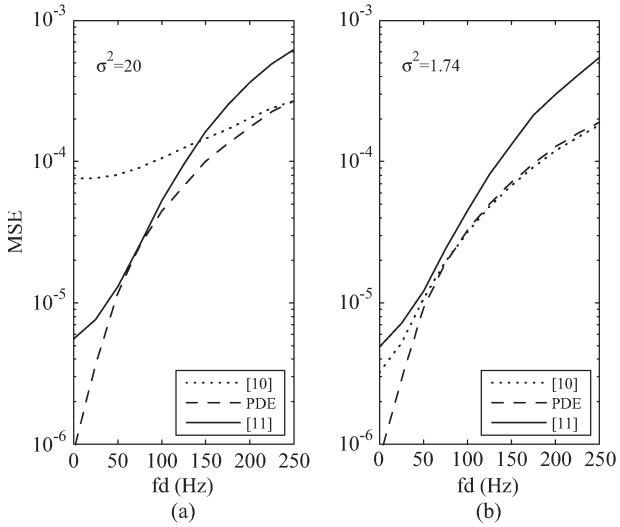

Fig. 5. MSE versus Doppler frequency over frequency-selective channels: SNR = 40 dB.

range of Doppler shifts. The estimator proposed in [11] is considered here because it is known for its robustness in frequency-selective channels. Fig. 5(a) considers the severe frequency-selective channel model, i.e., channel 3. As depicted in this figure, the PDE outperforms the estimators in [10] and [11] for the entire range of f_d. Although the performance difference between the PDE and the estimator in [10] decreases as f_d increases, they converge only at very high values of f_d. Moreover, the performance difference at low and moderate f_d values is substantial. The system reported in [11] demonstrated higher robustness against frequency selectivity as compared with that in [10]; however, it is more sensitive to Doppler shifts. Fig. 5(b) considers the case of mild frequency selectivity, i.e., channel 1. As can be noted from this figure, the PDE outperforms the estimator in [11] for the entire range of f_d, but it outperforms that in [10] only at low values of f_d. At moderate and high f_d values, the MSE of the PDE becomes slightly larger than the MSE of the system reported in [10]. Therefore, this figure confirms the robustness of the PDE under both frequency-selective and time-selective channels.

V. Conclusion

In this paper, we have presented a hybrid time–frequency-domain technique for blind CFO estimation of OFDM systems with CM data symbols. The performance of the proposed estimator has been evaluated over various channel models, including static and time-varying frequency-selective channels. Simulation results have confirmed that the proposed estimator outperforms the considered estimators over the entire range of SNRs. However, the MSE difference becomes more significant at high SNRs because the MSE of the proposed system does not suffer from the saturation that appears at high SNRs for other estimators. Additionally, the proposed estimator can be considered as a low-complexity system because it requires only three trial values to find the CFO estimate.

Appendix

In this Appendix, we present the derivation of the cost function given in (14). In the development of the derivation, we consider the noise-free case of (7) and assume that no averaging is used, i.e., $L = 1$.

By substituting (3) in (7), we obtain

$$s_k(l) = \frac{e^{j\frac{2\pi}{N}\epsilon l(N+N_g)}}{N} \sum_{i=0}^{N-1} \tilde{s}_i(l) \sum_{n=0}^{N-1} e^{j\frac{2\pi}{N}n(i+\delta-k)} \tag{20}$$

where $\delta = \epsilon - \hat{\epsilon}$, and $\tilde{s}_i(l) \triangleq d_i(l)H_i(l)$. Expanding (12) gives

$$J(\tilde{\epsilon}) = \sum_{k=0}^{N-1} |s_k(l)|^4 + \sum_{k=0}^{N-1} |s_k(l-1)|^4 - 2\sum_{k=0}^{N-1} |s_k(l)|^2 |s_k(l-1)|^2 . \tag{21}$$

Substituting (20) in the first term in (21) gives

$$\begin{aligned}\sum_{k=0}^{N-1} |s_k(l)|^4 &= \frac{1}{N^4} \sum_{i_1,i_2,c_1,c_2=0}^{N-1} \tilde{s}_{i_1}(l)\tilde{s}^*_{i_2}(l)\tilde{s}_{c_1}(l)\tilde{s}^*_{c_2}(l) \\ &\quad \times \sum_{n_1,n_2,m_1,m_2=0}^{N-1} e^{j\frac{2\pi}{N}\delta\lambda} e^{j\frac{2\pi}{N}(n_1 i_1 - n_2 i_2 + m_1 c_1 - m_2 c_2)} \\ &\quad \times \sum_{k=0}^{N-1} e^{-j\frac{2\pi k}{N}\lambda}\end{aligned} \tag{22}$$

where $\lambda = n_1 - n_2 + m_1 - m_2$. Note that

$$\sum_{k=0}^{N-1} e^{-j\frac{2\pi}{N}k\lambda} = \begin{cases} N, & \lambda = N, 0, -N \\ 0, & \text{otherwise.} \end{cases} \tag{23}$$

Thus, (22) can be simplified to (24), shown at the bottom of the page, where $C_1(l)$ is a real constant independent of δ that can be obtained by substituting $\lambda = 0$ in (22). Now, define

$$\begin{aligned}\Omega &\triangleq \{i_1, i_2, c_1, c_2\} \\ \Omega_1 &\triangleq \{\Omega \,|\, i_1 = i_2 \text{ or } c_1 = c_2\} \\ \Omega_2 &\triangleq \{\Omega \,|\, i_1 \neq i_2 \text{ and } c_1 \neq c_2\}\end{aligned}$$

where the indices i_1, i_2, c_1, $c_2 \in \{0, 1, \ldots, N-1\}$, $\Omega = \Omega_1 \cup \Omega_2$, and $\Omega_1 \cap \Omega_2 = \emptyset$. Therefore, (24) can be expressed as

$$\sum_{k=0}^{N-1} |s_k(l)|^4 = \frac{2}{N^3}\mathrm{Re}\left\{e^{-j2\pi\delta} B_{\Omega_1}(l)\right\} + \frac{2}{N^3}\mathrm{Re}\left\{e^{-j2\pi\delta} B_{\Omega_2}(l)\right\} + C_1(l) \tag{25}$$

$$\sum_{k=0}^{N-1} |s_k(l)|^4 = \frac{2}{N^3}\mathrm{Re}\left\{e^{-j2\pi\delta} \sum_{i_1,i_2,c_1,c_2=0}^{N-1} \tilde{s}_{i_1}(l)\tilde{s}^*_{i_2}(l)\tilde{s}_{c_1}(l)\tilde{s}^*_{c_2}(l) \times \sum_{n_1=0}^{N-1} \sum_{n_2=n_1+1}^{N-1} \sum_{m_1=0}^{n_2-n_1-1} e^{j\frac{2\pi}{N}n_1(i_1-c_2)} e^{-j\frac{2\pi}{N}n_2(i_2-c_2)} e^{-j\frac{2\pi}{N}m_1(c_1-c_2)} \right\} + C_1(l) \tag{24}$$

where

$$B_{\Psi}(l) = \sum_{\substack{i_1,i_2,c_1,c_2=0 \\ i_1,i_2,c_1,c_2\in\Psi}}^{N-1} \tilde{s}_{i_1}(l)\tilde{s}^*_{i_2}(l)\tilde{s}_{c_1}(l)\tilde{s}^*_{c_2}(l) \sum_{n_1=0}^{N-1}\sum_{n_2=n_1+1}^{N-1} \times \sum_{m_1=0}^{n_2-n_1-1} e^{j\frac{2\pi n_1}{N}(i_1-c_2)} e^{-j\frac{2\pi n_2}{N}(i_2-c_2)} e^{-j\frac{2\pi m_1}{N}(c_1-c_2)} \quad (26)$$

and $\Psi \in \{\Omega_1, \Omega_2\}$. Similarly

$$\sum_{k=0}^{N-1} |s_k(l-1)|^4 = \frac{2}{N^3}\mathrm{Re}\left\{e^{-j2\pi\delta} B_{\Omega_1}(l-1)\right\} + \frac{2}{N^3}\mathrm{Re}\left\{e^{-j2\pi\delta} B_{\Omega_2}(l-1)\right\} + C_1(l-1). \quad (27)$$

The last term can be expressed as

$$\sum_{k=0}^{N-1} |s_k(l)|^2 |s_k(l-1)|^2 = \frac{2}{N^3}\mathrm{Re}\left\{e^{-j2\pi\delta} D_{\Omega_1}(l)\right\} + \frac{2}{N^3}\mathrm{Re}\left\{e^{-j2\pi\delta} D_{\Omega_2}(l)\right\} + C_2(l) \quad (28)$$

where

$$D_{\Psi}(l) = \sum_{\substack{i_1,i_2,c_1,c_2=0 \\ i_1,i_2,c_1,c_2\in\Psi}}^{N-1} \tilde{s}_{i_1}(l)\tilde{s}^*_{i_2}(l)\tilde{s}_{c_1}(l-1)\tilde{s}^*_{c_2}(l-1) \times \sum_{n_1=0}^{N-1}\sum_{n_2=n_1+1}^{N-1}\sum_{m_1=0}^{n_2-n_1-1} e^{j\frac{2\pi}{N}n_1(i_1-c_2+1)} \times e^{-j\frac{2\pi}{N}n_2(i_2-c_2+1)} e^{-j\frac{2\pi}{N}m_1(c_1-c_2)}. \quad (29)$$

Substituting (25), (27), and (28) in (21) gives

$$J(\tilde{\epsilon}) = \frac{2}{N^3}\mathrm{Re}\left\{e^{-j2\pi\delta}\left(B_{\Omega_1}(l) + B_{\Omega_1}(l-1) - 2D_{\Omega_1}(l)\right)\right\} + \frac{2}{N^3}\mathrm{Re}\left\{e^{-j2\pi\delta}\left(B_{\Omega_2}(l) + B_{\Omega_2}(l-1) - 2D_{\Omega_2}(l)\right)\right\} + C_1(l) + C_1(l-1) - 2C_2(l). \quad (30)$$

To simplify (30), we define $\Omega_{1,a} \triangleq \{i_1, i_2, c_1, c_2 \,|\, i_1 \neq i_2 \text{ and } c_1 = c_2\}$, $\Omega_{1,b} \triangleq \{i_1, i_2, c_1, c_2 \,|\, i_1 = i_2 \text{ and } c_1 \neq c_2\}$, and $\Omega_{1,c} \triangleq \{i_1, i_2, c_1, c_2 \,|\, i_1 = i_2 \text{ and } c_1 = c_2\}$. Note that $\Omega_1 = \Omega_{1,a} \cup \Omega_{1,b} \cup \Omega_{1,c}$, $\Omega_{1,a} \cap \Omega_{1,b} = \emptyset$, $\Omega_{1,a} \cap \Omega_{1,c} = \emptyset$, and $\Omega_{1,b} \cap \Omega_{1,c} = \emptyset$. Therefore, $B_{\Omega_1} = B_{\Omega_{1,a}} + B_{\Omega_{1,b}} + B_{\Omega_{1,c}}$, and $D_{\Omega_1} = D_{\Omega_{1,a}} + D_{\Omega_{1,b}} + D_{\Omega_{1,c}}$. Following the same procedure as in [10]

$$D_{\Omega_{1,a}}(l) \approx \sum_{\substack{i_1,i_2,c_1,c_2=0 \\ i_1,i_2,c_1,c_2\in\Omega_{1,a}}}^{N-1} \tilde{s}_{i_1}(l)\tilde{s}^*_{i_2}(l)\tilde{s}_{c_1}(l-1)\tilde{s}^*_{c_2}(l-1) \times f(i_1,i_2,c_1,c_2) \quad (31)$$

where

$$f(i_1,i_2,c_1,c_2) \triangleq \sum_{n_1=0}^{N-1}\sum_{n_2=n_1+1}^{N-1}\sum_{m_1=0}^{n_2-n_1-1} e^{j\frac{2\pi}{N}n_1(i_1-c_2)} \times e^{-j2\pi N n_2(i_2-c_2)} e^{-j\frac{2\pi}{N}m_1(c_1-c_2)}. \quad (32)$$

In (31), $c_1 = c_2$; thus, both variables can be replaced by a common variable c

$$D_{\Omega_{1,a}}(l) \approx \sum_{\substack{i_1,i_2,c=0 \\ i_1,i_2,c\in\Omega_{1,a}}}^{N-1} \tilde{s}_{i_1}(l)\tilde{s}^*_{i_2}(l)\left|H_c(l)\right|^2 f(i_1,i_2,c). \quad (33)$$

The term $|H_c(l)|^2$ is obtained using the assumption in (11), where $\tilde{s}_c(l-1)\tilde{s}^*_c(l-1) = |H_c(l-1)|^2 \approx |H_c(l)|^2$. Using the same procedure, it can be shown that

$$B_{\Omega_{1,a}}(l) = \sum_{\substack{i_1,i_2,c=0 \\ i_1,i_2,c\in\Omega_{1,a}}}^{N-1} \tilde{s}_{i_1}(l)\tilde{s}^*_{i_2}(l)|H_c(l)|^2 f(i_1,i_2,c). \quad (34)$$

Hence, $B_{\Omega_{1,a}}(l) \approx D_{\Omega_{1,a}}(l)$. By applying the same approach to all other cases, we obtain $B_{\Omega_{1,b}}(l) \approx D_{\Omega_{1,a}}(l)$, $B_{\Omega_{1,c}}(l) \approx D_{\Omega_{1,c}}(l)$, $B_{\Omega_{1,a}}(l-1) \approx D_{\Omega_{1,b}}(l)$, $B_{\Omega_{1,b}}(l-1) \approx D_{\Omega_{1,b}}(l)$, and $B_{\Omega_{1,c}}(l-1) \approx D_{\Omega_{1,c}}(l)$. Therefore, $B_{\Omega_1}(l-1) + B_{\Omega_1}(l) \approx 2D_{\Omega_1}(l)$, and (30) can be reduced to

$$J(\tilde{\epsilon}) \approx A\cos(2\pi\delta) + C \quad (35)$$

where A and C are real constants

$$A = -2\left[B_{\Omega_2}(l) + B_{\Omega_2}(l-1) - 2D_{\Omega_2}(l)\right]/N^3 > 0$$

$$C = C_1(l) + C_1(l-1) - 2C_2(l).$$

REFERENCES

[1] Y. Li and G. Stüber, *Orthogonal Frequency Division Multiplexing for Wireless Communications*. New York: Springer-Verlag, 2006.

[2] Radio Broadcasting Systems; Digital Audio Broadcasting (DAB) to Mobile, Portable and Fixed Receivers, Eur. Telecommun. Stand. 300 401, 1997.

[3] Digital Video Broadcasting (DVB); Framing Structure, Channel Coding and Modulation for Digital Terrestrial Television, Eur. Stand. EN 300 744 V1.1.2 (1997-08).

[4] A. Al-Dweik, R. Hamila, and M. Renfors, "Blind estimation of large carrier frequency offsets in wireless OFDM systems," *IEEE Trans. Veh. Technol.*, vol. 56, no. 2, pp. 965–968, Mar. 2007.

[5] A. Al-Dweik, "Robust non data-aided frequency offset estimation technique for OFDM systems in Rayleigh fading channels," in *Proc. IEEE PIMRC*, 2004, pp. 1365–1369.

[6] P. Moose, "A technique for orthogonal frequency division multiplexing frequency offset correction," *IEEE Trans. Commun.*, vol. 42, no. 10, pp. 2908–2914, Oct. 1994.

[7] J. van de Beek, M. Sandell, and P. Börjesson, "ML estimation of timing and frequency offset in OFDM systems," *IEEE Trans. Signal Process.*, vol. 45, no. 7, pp. 1800–1805, Jul. 1997.

[8] A. Al-Dweik, B. Sharif, and R. Shubair, "Robust frequency offset estimator for OFDM with general constellation," *IET Electron. Lett.*, vol. 44, no. 16, pp. 980–981, Jul. 2008.

[9] Y. Yao and G. B. Giannakis, "Blind carrier frequency offset estimation in SISO, MIMO and multiuser OFDM systems," *IEEE Trans. Commun.*, vol. 53, no. 1, pp. 173–183, Jan. 2005.

[10] X. Zeng and A. Ghrayeb, "A blind carrier frequency offset estimation scheme for OFDM systems with constant modulus signaling," *IEEE Trans. Commun.*, vol. 56, no. 7, pp. 1032–1037, Jul. 2008.

[11] J. Lee, H. Lou, D. Toumpakaris, and J. M. Cioffi, "A blind frequency tracking algorithm for OFDM transmission over frequency selective channels," in *Proc. IEEE VTC*, 2004, pp. 578–582.

[12] J. Lin, "A frequency offset estimation technique based on frequency error characterization for OFDM communications on multipath fading channels," *IEEE Trans. Veh. Technol.*, vol. 56, no. 3, pp. 1209–1222, May 2007.

[13] T. S. Rappaport, *Wireless Communications: Principles and Practice*. Englewood Cliffs, NJ: Prentice-Hall, 1998.